Higher-order and $E2$ effects in medium energy ^{8}B breakup

J. Mortimer, I. J. Thompson, and J. A. Tostevin
Department of Physics, School of Physics and Chemistry, University of Surrey, Guildford, Surrey GU2 7XH, United Kingdom
(Received 11 April 2002; published 20 June 2002)

Longitudinal momentum distributions of ^{7}Be fragments following the dissociation of ^{8}B on heavy, highly charged target nuclei show forward-aft asymmetries, the result of interference of electric quadrupole ($E2$) transitions with the dominant $E1$ excitation process. These asymmetries can therefore be used to gain insight into the $E2$ contributions to the breakup process. To assess the sensitivity of these $E2$ interference terms to the assumed reaction mechanism, in particular, the role of higher-order coupling effects at medium energies, coupled discretized continuum channels (CDCC) calculations are carried out for ^{8}B breakup at 44 and 81 MeV/nucleon on heavy targets. The effects of higher-order processes due to both Coulomb and nuclear breakup mechanisms can be estimated. In line with earlier work we find that the asymmetries produced by the calculations are reduced when including the higher-order couplings, reflecting an effective quenching of the $E2$ contributions. The full CDCC calculations show less asymmetry than the available experimental data, suggesting that the structure or reaction model now contains insufficient $E2$ strength. This contrasts with the results of lowest-order reaction theories that conclude that the ^{8}B model $E2$ amplitudes are too large.

DOI: 10.1103/PhysRevC.65.064619 PACS number(s): 24.10.Eq, 25.60.Gc, 25.70.De, 27.20.+n

I. INTRODUCTION

The properties of light, weakly bound nuclei have been studied in nuclear physics for a number of years. Of recent interest is the Coulomb breakup of these nuclei, which can be used to gain information about the inverse capture reactions that are important in nuclear astrophysics [1]. Charged particle capture reactions at stellar temperatures have very small cross sections due to the Coulomb barrier, therefore direct measurements of these cross sections are difficult. However, breakup reactions of light nuclei in the Coulomb field of a high Z nucleus have large cross sections at projectile incident energies of 10–100 MeV/nucleon. Measurements of the projectile fragments emerging at extremely forward angles, and having experienced small momentum transfers, allow the interactions between the projectile fragments at low relative energies to be investigated.

An important proton capture reaction is ^{7}Be$(p,\gamma)^8$B. Determining its reaction rate at solar temperatures is relevant to the solar neutrino problem, as the neutrinos produced in ^{8}B decay are the major contributor to the high energy neutrino flux from the Sun. Several attempts have been made to measure the ^{7}Be(p,γ) cross section directly [2–9], but at proton energies considerably higher than those found at solar temperatures, which are typically 15–20 keV. Analyses of these data in terms of the astrophysical S factor have then been extrapolated to low energies to extract the zero energy S factor $S_{17}(0)$ [2,3]. Difficulties in measuring the capture cross section, and uncertainties in the subsequent extrapolation, mean that the value of $S_{17}(0)$ is still not known to sufficient accuracy.

Indirect studies of the ^{7}Be(p,γ) cross section have also been made by performing Coulomb dominated ^{8}B breakup experiments on heavy target nuclei such as Pb and Ag [10–14]. However, a complication in the interpretation of ^{8}B breakup measurements is that, as well as the $E1$ transitions that completely dominate the capture process, $E2$ transitions may also contribute to the breakup cross section.

Theoretical predictions [15–18] have been made concerning the importance of $E2$ transitions in ^{8}B Coulomb breakup assuming different structure models. In these, the breakup differential cross sections were expressed as a function of (a) the proton-^{7}Be center of mass (c.m.) scattering angle, and (b) their relative energy, in an attempt to reproduce the data of Motobayashi *et al.* [10,11]. However, these observables are not well suited to gauge the $E2$ strength since their $E1$ and $E2$ contributions are incoherent. There have therefore been efforts to measure observables sensitive to $E1/E2$ interference.

In a series of recent experiments Davids *et al.* [13,14,19] have measured the parallel momentum distributions $d\sigma/dp_\parallel$ of the ^{7}Be fragments produced in the breakup of ^{8}B on heavy nuclei at 40–80 MeV/nucleon. These ^{7}Be fragment parallel momentum distributions are a particularly sensitive indicator of competing $E1$ and $E2$ dominated breakup pathways, showing strong interference effects even in leading order [19,20]. Using first-order semiclassical (Coulomb excitation) theory, the $E2$ amplitude from a simple single-particle ^{8}B structure model [18,21] had to be reduced by a factor of 0.7 in order to reproduce the measured interference in the 44.1-MeV data [13,19]. Higher-order effects were suggested as being the source of this reduction. This supposition is supported also by earlier [18,22] time-dependent calculations of the effects of higher-order coupling contributions, in ^{8}B+Au at 41 MeV/nucleon, and also by semiclassical calculations [23] for a similar reaction. These showed a reduced level of interference, i.e., an effective suppression of $E2$ strength within that higher-order analysis. Such time-dependent formulations of higher-order effects have been refined considerably, meanwhile, using the efficiency of Lagrange mesh techniques [24], although these have not yet been applied to parallel momentum distribution calculations for the ^{8}B system. This earlier work is sufficient to indicate that higher-order effects, and the assumed reaction mechanism may play a significant rôle in the breakup process and

so needs to be considered carefully when assessing the $E2$ contribution to breakup.

Nuclear interaction induced breakup may also contribute to the measured cross section. First-order Coulomb breakup calculations for the ^{8}B+Ag system at 44 MeV/nucleon [14] fail to reproduce the widths of the measured parallel momentum distributions. It was suggested this may be due to nuclear contributions, which were not taken into account in that analysis, and which are also difficult to include to all orders in the time-dependent methods of Refs. [18,25]. Despite the peripheral nature of the reactions, selected by the detection of only those ^{7}Be fragments emerging at very forward angles, nuclear interactions between the projectile and target are possible, due to the highly extended nature of the ^{8}B wave function.

We note also a recent coupled discretized continuum channels (CDCC) study [26] of data for the ^{8}B+^{58}Ni breakup reaction at low energy, 26 MeV [27]. At this near Coulomb barrier energy the rôles of both the Coulomb and nuclear interactions were strong, as were the effects of $E1$, $E2$, and $E3$ electric multipole transitions. These data included the ^{7}Be final state energy distributions measured at several laboratory angles which, like the $p_{\|}$ distributions, are strongly affected by interference between breakup partial waves. The CDCC calculations were able to reproduce the full data set within the accuracy of the measurements and showed only very minor sensitivity to the parameters of the model, such as the proton-target potential. In particular, no adjustment of the structure model $E\lambda$ strengths, to be discussed here, were found to be necessary in that analysis. Moreover, the $E2$ contributions were large.

In this paper we present the results of a CDCC coupled channels analysis of the breakup of ^{8}B on Pb and Ag targets at 44 and 81 MeV/nucleon. The calculations include both the Coulomb and nuclear interactions of the projectile fragments with the target as well as treating the ^{8}B excitations to all orders. We highlight the importance of higher-order effects in the breakup by comparison of the all-order CDCC results with first-order distorted waves Born approximation (DWBA) calculations. We also compare the calculations with the measured parallel momentum distributions of Davids *et al.* [14] in an attempt to clarify the $E2$ contribution to the breakup cross section and its sensitivity to the assumed reaction model.

II. STRUCTURE MODELS

The ground state (g.s.) of ^{8}B has $J^\pi=2^+$, the dominant configuration being a proton in a $0p_{3/2}$ orbit coupled to the ^{7}Be($3/2^-$, g.s.) core. Several single-particle structure models have been proposed [16,18,28–32] based on one-body potential models to bind ^{8}B. These are compared in Ref. [33]. In the model of Esbensen and Bertsch [18] the potential well depths in the $p+^7$Be(J^π) channels are also adjusted to reproduce the known 1^+ and 3^+ ^{8}B* resonances. These modified depths act as an effective spin-dependent interaction with the ^{7}Be core.

Here we will assume the simplest model of a pure $p_{3/2}$ valence proton orbital around a spectator core with uncoupled spins and unit spectroscopic factor. In doing so we neglect (a) possible small $p_{1/2}$ proton configurations, (b) excited ^{7}Be core components in the wave function, and (c) the physical differences in the energies of the 2^+(g.s.) and 1^+ and 3^+ resonances. We believe that careful all-order calculations, even in this simple model space, are valuable to help identify the disagreements, if any, of such a model with the available data.

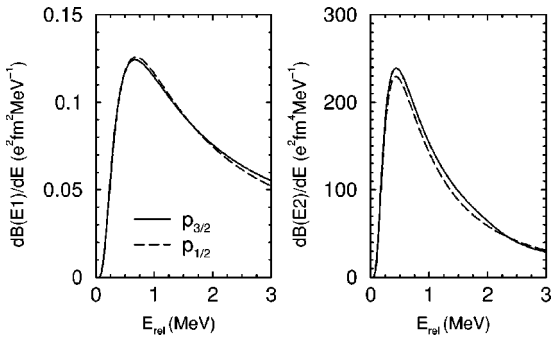

FIG. 1. Single-particle electric dipole (left) and quadrupole (right) strength functions for Coulomb breakup of ^{8}B$\rightarrow^7$Be$+p$ as a function of relative energy of the fragments.

Concerning the points above: (a) the microscopic shell model calculates a [$p_{3/2}\times^7$Be(g.s.)] spectroscopic factor close to unity [34,35]. A very recent analysis of proton removal data from ^{8}B, at energies between 142 MeV/nucleon–1.44 GeV/nucleon, is also consistent with a measured spectroscopic factor of one [36]. Calculations that treat ^{8}B as a ($\alpha+^3$He$+p$) three-body system, however, predict a significantly lower spectroscopic factor for this [$p_{3/2}\times^7$Be(g.s.)] configuration, of order 0.7 [37]. To examine the possible influence of $p_{1/2}$ configurations in a single-particle model, we compare in Fig. 1 the $E1$ and $E2$ strength distributions for $p_{3/2}$ (solid line) and $p_{1/2}$ (dashed line) valence proton orbitals. We find very little difference in the dipole strength functions. A more noticeable difference is seen in the quadrupole strength function for the two configurations for relative energies from 0 to 2 MeV, but even here, because the $p_{1/2}$ probability is small, the likely errors on the breakup calculations are probably of order 1%.

(b) We neglect both dynamical excitation of ^{7}Be and any ^{7}Be core excited component in the ^{8}B ground state. The latter is quantified by a recent experiment at the GSI [38] that measured a (13±3)% branch from the ^{7}Be($1/2^-$) excited state following proton removal from the ^{8}B ground state by a ^{12}C target. This excited core component is neglected in the present breakup model.

(c) We neglect the splitting of the 2^+ and 1^+ states, and so do not include the 1^+ (0.6 MeV) resonance. This resonance produces only a very narrow peak in the $M1$ and $E2$ strength functions [18], which are otherwise the same as those of Fig. 1. At the beam energies of interest here the $M1$ transition is in any case very small (approximately 3%) compared to the $E1$ and $E2$ transitions.

We conclude that our neglect of dynamical coupling to the core degrees of freedom will induce small errors in breakup observables for low and medium energy breakup experi-

ments. For the present we treat the core as a spectator in the breakup process. Accurate calculations within this model space, in comparison with data, can then be used to assess the likely importance of the approximations made.

In our spectator core model, the proton $p_{3/2}$ initial state is computed in a (trivially) modified version of the Esbensen and Bertsch [18] model. A single spherical Woods-Saxon plus spin-orbit potential, with geometry parameters $r_0 = 1.25$ fm, $a = 0.52$ fm, and $V_{so} = 4.898$ MeV, is used throughout for the core-proton nuclear interaction in the ground and all continuum states. A central well depth $V_0 = 44.97$ MeV reproduces the correct proton g.s. separation energy of 0.137 MeV.

III. COUPLED DISCRETIZED CONTINUUM CHANNELS BREAKUP THEORY

In this section we outline the necessary CDCC formalism [39,40] for analyzing the parallel momentum distributions of the core fragments in ^{8}B elastic breakup. The CDCC calculates an approximate description of the projection of the full many-body wave function onto the ground states of the target and core nuclei. The target is assumed here to have spin zero. The breakup is of a two-body projectile p (^{8}B) with charge Z_p, mass m_p, incident on a target nucleus of charge Z_t, and mass m_t. The projectile consists of a core of mass m_c, charge Z_c, and a valence proton of mass m_v.

The projectile interacts with the target through effective core- and valence proton-target tidal interactions $V_{ct}(\vec{R}_c)$ and $V_{vt}(\vec{R}_v)$ with $\vec{R}_c$ and $\vec{R}_v$ the core- and proton-target separations. These potentials include both the nuclear and Coulomb interactions. We denote by $\vec{R}$ the position of the c.m. of the core and proton relative to the target and by $\vec{r}$ the position of the proton relative to the core.

The core particle in our spectator model can be assumed spinless, while the proton has spin $s(=1/2)$ and projection σ. These particles are assumed structureless. The total angular momentum of the projectile ground state is I, with projection M, in which the relative orbital angular momentum of the two constituents is l_0 and their separation energy is $\mathcal{E}_0$ (>0). The incident wave number of the projectile in the c.m. frame of the projectile and target is $\vec{K}_0$ and the coordinate z axis is chosen in the incident beam direction.

The CDCC treatment now couples the incident projectile state (I,M), in all orders, to selected breakup configurations (I',M') of the core and proton, with relative orbital angular momentum l. This continuum of breakup states, in each significant spin-parity excitation I', is further grouped into a number $\mathcal{N}(I')$ of representative energy intervals or bins. In each bin i, representing states with wave numbers on the interval $[k_{i-1} \to k_i]$, a square integrable bin state $\hat{\phi}_\alpha, \alpha \equiv [i,(ls)I']$ is constructed [26] as a weighted superposition of the scattering states in that interval. The bins in each I' channel extend up to a maximum relative energy $\mathcal{E}_{max}$. The actual CDCC model space used is detailed in Sec. IV.

A. Construction of continuum bin states

For each bin interval, with width $\Delta k_i = [k_i - k_{i-1}]$, the representative bin state is, explicitly,

$$\hat{\phi}_\alpha^{M'}(\vec{r}) = [Y_l(\hat{r}) \otimes \mathcal{X}_s]_{I'M'} u_\alpha(r)/r. \tag{1}$$

The radial functions u_α are square integrable superpositions, with weight functions $g_\alpha(k)$,

$$u_\alpha(r) = \sqrt{\frac{2}{\pi N_\alpha}} \int_{k_{i-1}}^{k_i} g_\alpha(k) f_\alpha(k,r)\, dk, \tag{2}$$

of the scattering states $f_\alpha(k,r)$, eigenstates of the $c+p$ relative motion Hamiltonian H_p. The normalization factor is $N_\alpha = \int_{k_{i-1}}^{k_i} |g_\alpha(k)|^2\, dk$. The f_α are defined here such that, for $r \to \infty$,

$$f_\alpha(k,r) \to [\cos\delta_\alpha(k) F_l(kr) + \sin\delta_\alpha(k) G_l(kr)], \tag{3}$$

where k belongs to bin α and F_l and G_l are the regular and irregular partial wave Coulomb functions. So the f_α are real when using a real core-proton two-body interaction. Energy conservation connects the wave numbers K_α of the c.m. of the fragments in bin state α and the corresponding bin state excitation energies $\hat{\mathcal{E}}_\alpha = \langle \hat{\phi}_\alpha | H_p | \hat{\phi}_\alpha \rangle$. For non-$s$-wave bins we used $g_\alpha(k) = 1$. For the s-wave bins we used $g_\alpha(k) = k$ that aids the interpolation of the three-body transition amplitude near the breakup threshold in Eq. (4).

These bin states $\hat{\phi}_\alpha$ provide an orthonormal relative motion basis for the coupled channels solution of the three-body wave function. The bins and their coupling potentials $\langle \hat{\phi}_\alpha | V_{ct} + V_{vt} | \hat{\phi}_\beta \rangle$ are constructed, and the coupled equations are solved, either exactly or iteratively, using the coupled channels code FRESCO [41]. Using the iterative method, first-order DWBA solutions can be found as the approximate solutions [42,43] of the CDCC equations, with these same couplings, but then each ground state to bin coupling acts only once. The core and proton interactions with the target are expanded to multipole order λ.

The coupled equations solution generates (effective two-body) transition amplitudes $\hat{T}^\alpha_{M'M}(\vec{K}_\alpha)$, already summed over projectile-target partial waves, for populating each bin state I',M' from initial state I,M, as a function of the angle of the center of mass of the emerging excited projectile in the c.m. frame. These amplitudes are expressed in a coordinate system with x axis in the plane of $\vec{K}_0$ and $\vec{K}_\alpha$. For a general x-coordinate axis the coupled channels amplitudes must subsequently be multiplied by $\exp(i[M-M']\phi_K)$, with ϕ_K referred to the chosen x axis.

B. Three-body breakup observables

The relationship of the CDCC coupled channels bin state inelastic amplitudes $\hat{T}^\alpha_{M'M}(\vec{K}_\alpha)$ to the physical breakup transition amplitudes $T_{\sigma:M}(\vec{k},\vec{K})$ from initial state I,M to a three-body continuum final state is discussed in detail in Ref. [26]. This is needed to make predictions for the detection

geometries considered here, since each detector configuration and detected fragment energy involves a distinct final state c.m. wave vector $\vec{K}$, breakup energy $\mathcal{E}_k$, and relative motion wave vector $\vec{k}$.

The three-body breakup T matrix can be written [26]

$$T_{\sigma:M}(\vec{k},\vec{K}) = \frac{(2\pi)^{3/2}}{k} \sum_{\alpha\nu} (-i)^l (l\nu s\sigma | I'M') \exp[i\overline{\delta}_\alpha(k)] \times Y_l^\nu(\hat{k}) g_\alpha(k) T_{M'M}(\alpha,\vec{K}). \quad (4)$$

Here $\overline{\delta}_\alpha(k)$ is the sum of the nuclear and Coulomb proton-core relative motion phase shifts in excited state I', and the $T_{M'M}(\alpha,\vec{K})$ are interpolated from the coupled channels amplitudes $\hat{T}^\alpha_{M'M}(\vec{K}_\alpha)$ available on the chosen K_α and θ_{K_α} grid. Explicitly,

$$T_{M'M}(\alpha,\vec{K}) = \exp(i[M-M']\phi_K)[\hat{T}^\alpha_{M'M}(\vec{K})/\sqrt{N_\alpha}], \quad (5)$$

where the value of the bracketed term on the right hand side is interpolated from the coupled channels solution. The number of bin states used to describe each I' excitation must allow an accurate interpolation of these amplitudes. The sum in Eq. (4) is taken over all bin states α that contain k.

The three-body amplitudes, Eq. (4), are used to compute the triple differential cross sections for breakup in the laboratory frame. If the energy or momentum of the core particle is measured then the relevant cross section is

$$\frac{d^3\sigma}{dE_c d\Omega_c d\Omega_v} = \frac{2\pi\mu_{pt}}{\hbar^2 K_0} \frac{1}{(2I+1)} \sum_{\sigma M} |T_{\sigma:M}(\vec{k},\vec{K})|^2 \rho(E_c,\Omega_c,\Omega_v), \quad (6)$$

where μ_{pt} is the projectile-target reduced mass and $\rho(E_c,\Omega_c,\Omega_v)$ is the three-body phase space factor, calculated here using nonrelativistic kinematics [44]. If $\vec{p}_c$, $\vec{p}_v$, and $\vec{p}_{tot}$ denote particular values of the detected core, proton, and total final state momenta in the laboratory frame, then the relevant breakup T-matrix elements have c.m. and relative wave vectors $\vec{K}$ and $\vec{k}$, where

$$\hbar\vec{K} = \vec{p}_v + \vec{p}_c - \frac{m_v+m_c}{m_v+m_c+m_t}\vec{p}_{tot}, \qquad \hbar\vec{k} = \frac{m_c}{m_v+m_c}\vec{p}_v - \frac{m_v}{m_v+m_c}\vec{p}_c. \quad (7)$$

The data under discussion here are the parallel momentum distributions of the core fragments and the cross sections must be integrated numerically over all directions of the unobserved proton. The core $d\sigma/dp_{c\|}$ differential cross sections are computed by writing, after $d\Omega_v$ integration, in the laboratory frame,

$$\frac{d\sigma}{d\vec{p}_c} = \frac{1}{m_c p_c} \frac{d^2\sigma}{dE_c d\Omega_c} \quad (8)$$

and then integrating over the experimentally specified angular acceptance and/or perpendicular momentum components of the core.

The phase-space and kinematical equations were also derived using relativitistic kinematics. Relativity was found to have no effect on the shape of the distributions, only on the $d\sigma/dp_{c\|}$ centroid position, and, to a much lesser extent, their overall magnitudes.

IV. CDCC CALCULATIONS

The CDCC method described in the preceding section is applied to forward going fragments following the breakup of ^{8}B on Pb and Ag targets at 44 and 81 MeV/nucleon. Parallel momentum distributions of ^{7}Be are calculated for comparison with the data from the recent experiments at the National Superconducting Cyclotron Laboratory (NSCL) at Michigan State University [14]. In Ref. [14] the ^{8}B breakup cross section, on a Pb target at 83 MeV/nucleon, was measured with high precision also as a function of the relative energy of the proton and ^{7}Be. The accompanying CDCC calculations [14] were able to reproduce this data rather precisely and without parameter variation (see Fig. 17 of Ref. [14]). As previously stated, however, these data are incoherent in the electric multipole contributions and, as the $E2$ contributions are much reduced at this higher energy, do not pose such a demanding test of the theory. The quality of agreement of the CDCC calculations with the data do, however, give a reasonable indication that the CDCC produces a good overall $E1$ strength. Our emphasis in the following is therefore the required $E2$ strength.

A. *CDCC* model space

The model space parameters for the CDCC calculations are defined as follows. For all spin/parity excitations I' the continuum is discretized up to a maximum relative energy of $\mathcal{E}_{max}=10$ MeV. The number of bins for each I' excitation were as follows: $1/2^+$ has 20 bins, $1/2^-$,$3/2^-$,$3/2^+$,$5/2^+$ each have ten bins, and $5/2^-$,$7/2^-$ each have five bins. The bins had evenly spaced k_i from $k=0$ to k_{max}. When constructing each bin state, the numerical integration over Δk_i in Eq. (2) uses 50 intervals. Multipoles up to $\lambda=2$ and a maximum radius of $r_{max}=60$ fm are used when constructing the coupling interactions. Including also the $\lambda=3$ multipole couplings made very little difference to the calculations at the incident energies of the NSCL experiments and we conclude that these $E3$ couplings are negligible.

For the motion of the projectile c.m. relative to the target, partial waves up to $L=10\,000$ and values of $R \leqslant R_{max}=1000$ fm are used to compute the relative motion wave functions in the coupled channels set, where these limits as well as r_{max} are sufficient for stable results. With increasing L, the partial-wave values are calculated at progressively larger intervals and the intermediate S-matrix elements are computed by interpolation. The ^{7}Be-target interaction used

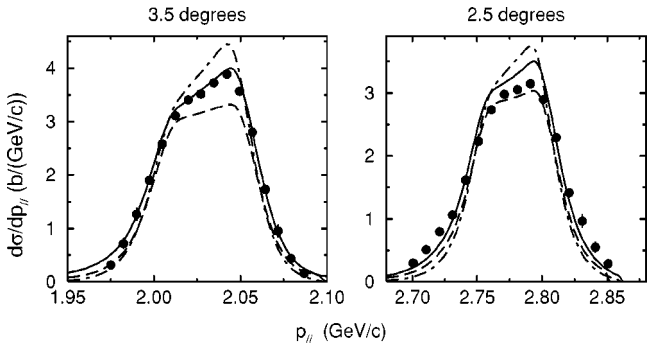

FIG. 2. Parallel momentum distribution of ^{7}Be from the breakup of ^{8}B on Pb at (i) 44 MeV/nucleon with $\theta_{max}=3.5°$ (left) and (ii) 81 MeV/nucleon with $\theta_{max}=2.5°$ (right). The curves are the results of CDCC (dashed) and first-order DWBA (solid) calculations using our assumed ^{8}B structure model. The dot-dashed curves are the results of first-order semiclassical (Coulomb excitation) calculations with the same $B(E\lambda)$ strength functions of Fig. 1.

in the calculations is that of Cook [45], obtained for ^{7}Li, and the proton-target interaction is calculated using the global nucleon optical potential parameter set of Becchetti and Greenlees [46], but without fragment-target spin-orbit interactions.

B. ^{7}Be parallel momentum distributions

Previous attempts to reproduce the measured ^{7}Be $d\sigma/dp_\parallel$, for ^{8}B on Pb at 44 MeV/nucleon, used the single-particle $B(E\lambda)$ distributions, Fig. 1, in semiclassical first-order perturbation theory calculations [19]. The structure-model-generated $E2$ strength was then scaled so as to reproduce the $E1/E2$ interference asymmetry seen in the data. Within this first-order approximation to the reaction dynamics the data required an $E2$ amplitude 0.7 times that given by the Esbensen and Bertsch structure model. We were able to reproduce these results in detail. The results of such semiclassical calculations are shown by the dot-dashed curves in Fig. 2, before any rescaling. The larger asymmetry of these calculations compared to the data is clear. An earlier nonperturbative, time-dependent calculation [18], however, produced $d\sigma/dp_\parallel$ distributions with a reduced asymmetry compared with first-order calculations for the same intrinsic structure and $B(E\lambda)$ inputs. This indicates that higher-order effects may play a significant rôle in the breakup process and that any deduced $E2$ strength from comparisons with data are reaction mechanism dependent.

Figure 2 shows the ^{7}Be parallel momentum distributions for the breakup of ^{8}B on Pb at 44 and 81 MeV/nucleon with maximum ^{7}Be acceptance angles of $\theta_{max}=3.5°$ and 2.5°, respectively. Distributions calculated using both the DWBA (solid lines) and CDCC (dashed lines) are shown. These are absolute predictions. The DWBA and CDCC calculations use the same structure model and model space. Comparison of the DWBA calculations with the semiclassical calculations (dot-dashed curves) shows that the quantum mechanical DWBA calculations, prior to the addition of higher-order effects, are already less asymmetric that the semiclassical results. These effects are a combination of the inclusion of

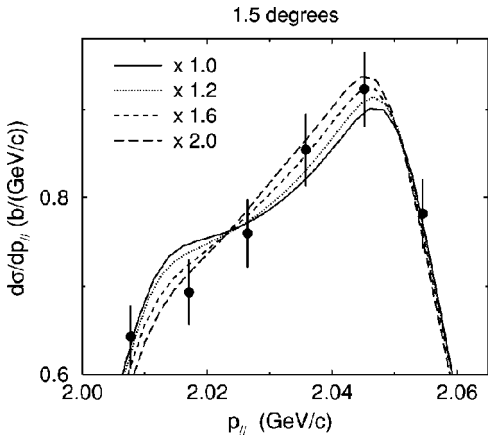

FIG. 3. Parallel momentum distribution of ^{7}Be from the breakup of ^{8}B on Ag at 44 MeV/nucleon with $\theta_{max}=1.5°$. The curves are results of CDCC calculations with the $\lambda=2$ multipole amplitudes scaled by the factors indicated.

nuclear interactions and the finite size of the target. The calculated $p_\parallel$ asymmetries from the CDCC method are reduced further from those of the DWBA, consistent with the only earlier comparison [18] of higher- and first-order calculations. Since the CDCC and DWBA calculations use the same ^{8}B structure model, the suppression of the $E1/E2$ interference shows a reduced effective $E2$ strength. This reduction is larger than is needed to describe the asymmetry of the data.

Figures 3 and 4 show how scaling of the $E2$ amplitude in the CDCC calculations changes the asymmetry in the central regions of the ^{7}Be parallel momentum distributions. The scaling means that all $\lambda=2$ multipole couplings are multiplied by the stated factor. As the object of this analysis is to reproduce the asymmetry of the measured distributions, the cross sections for each $E2$ scaling have had their overall magnitude renormalized (in the χ^2 fit sense) to the six central

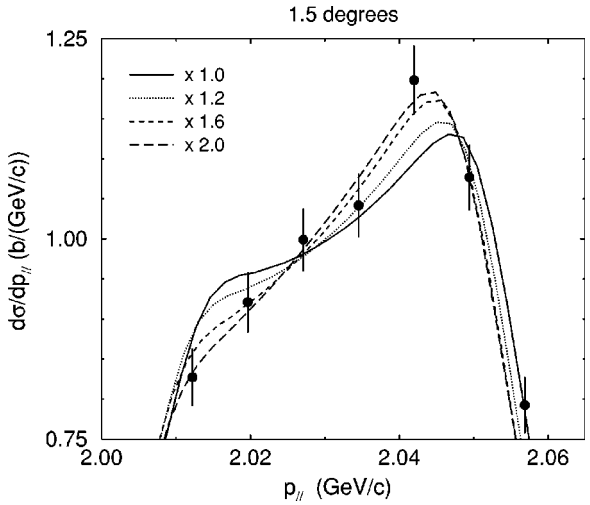

FIG. 4. Parallel momentum distribution of ^{7}Be from the breakup of ^{8}B on Pb at 44 MeV/nucleon with $\theta_{max}=1.5°$. The curves are results of CDCC calculations with the $\lambda=2$ multipole amplitudes scaled by the factors indicated.

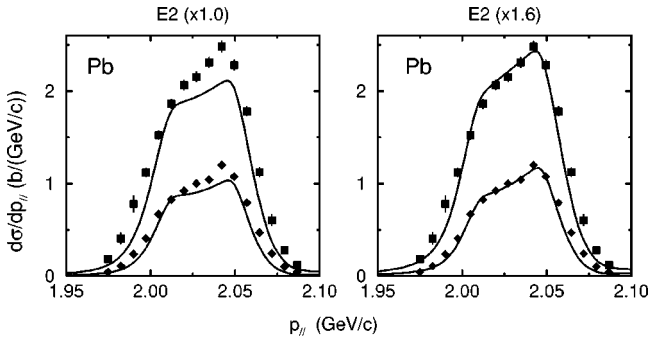

FIG. 5. Measured [19] and calculated parallel momentum distributions for ^{7}Be fragments, in the forward angle cones with $\theta_{max}=2.4°$ (filled squares) and $\theta_{max}=1.5°$ (filled diamonds), from ^{8}B breakup on a Pb target at 44.1 MeV/nucleon. The left panel shows the full CDCC calculations with the original ^{8}B model $E2$ strength. The right panel shows calculations in which all $\lambda=2$ multipole couplings have been scaled by a factor of 1.6.

data points of the measured distributions. The experimental uncertainty in the θ_{max} values in any case results in comparable uncertainties in the absolute magnitudes of the measured distributions, but not to their asymmetry. The renormalization allows a more direct comparison with the data. An $E2$ rescaling factor of 1.6 gives the best overall description of the data for the two energies and two targets.

The rescaling effects in the specific case of the Pb target at 44.1 MeV/nucleon are shown in Fig. 5. The original CDCC calculations are shown in the left panel and show insufficient interference (too shallow a slope) compared to the experimental data. Recall that the first-order theory gives curves which are too steep and require an $E2$ amplitude scaling of 0.7 to reproduce these data. On the contrary, the right panel shows that, within the CDCC, the $E2$ amplitude needs to be enhanced by a factor of order 1.6 to restore the measured interference effects.

Figures 6 and 7 show the ^{7}Be parallel momentum distributions for both the Ag and Pb targets at 44 and 81 MeV/

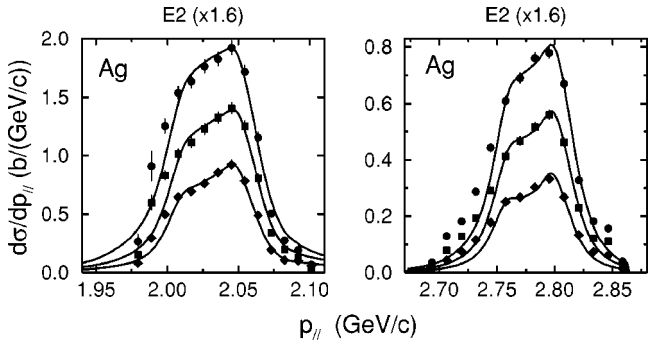

FIG. 6. Parallel momentum distributions of ^{7}Be from the breakup of ^{8}B on Ag at (i) 44 MeV/nucleon (left) into the forward angle cones with $\theta_{max}=1.5°$ (filled diamonds), $\theta_{max}=2.0°$ (filled squares), and $\theta_{max}=2.5°$ (filled circles) and (ii) 81 MeV/nucleon (right) into the forward angle cones with $\theta_{max}=0.75°$ (filled diamonds), $\theta_{max}=1.0°$ (filled squares), and $\theta_{max}=1.25°$ (filled circles). The curves are CDCC calculations in which all $\lambda=2$ multipole couplings have been scaled by a factor of 1.6.

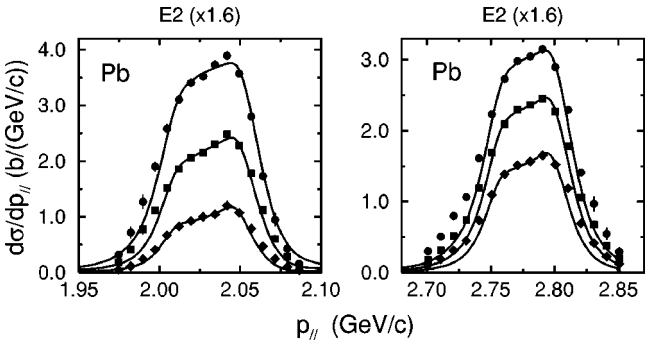

FIG. 7. Parallel momentum distributions of ^{7}Be from the breakup of ^{8}B on Pb at (i) 44 MeV/nucleon (left) into the forward angle cones with $\theta_{max}=1.5°$ (filled diamonds), $\theta_{max}=2.4°$ (filled squares), and $\theta_{max}=3.5°$ (filled circles) and (ii) 81 MeV/nucleon (right) into the forward angle cones with $\theta_{max}=1.5°$ (filled diamonds), $\theta_{max}=2.0°$ (filled squares), and $\theta_{max}=2.5°$ (filled circles). The curves are CDCC calculations in which all $\lambda=2$ multipole couplings have been scaled by a factor of 1.6.

nucleon for all available angular cuts. Each figure shows the CDCC results in which the $E2$ strength has been multiplied by 1.6. The distributions have been renormalized to the central six points for the 44 MeV/nucleon data and the central five points for the 81 MeV/nucleon data. At 44 MeV/nucleon, the scaling of 1.6 increases the asymmetry sufficiently to give a reasonable fit to the data for all angular cuts, perhaps with the exception of $\theta_{max}=3.5°$ case for the Pb target. Increasing the $E2$ amplitude by the same factor in the 81 MeV/nucleon calculations is seen to provide a good description of the asymmetry seen in that data also, although the importance of the $E2$ contributions, and indeed of the higher-order effects, fall with increasing incident energy.

V. SUMMARY AND CONCLUSIONS

In this paper the Coulomb breakup of ^{8}B on Ag and Pb targets at 44 and 81 MeV/nucleon has been investigated. The CDCC method is used to calculate the triple differential breakup cross section and hence the ^{7}Be parallel momentum distributions produced in the breakup. $E1/E2$ interference results in an asymmetry in the $p_{\|}$ distributions and this asymmetry is used to try to understand both the importance of higher-order effects in the breakup process, and the implications for the effective $E2$ transition strength.

Through comparison with first-order DWBA calculations it is shown that higher-order effects suppress the $E1/E2$ interference, reducing the asymmetry seen in the calculated distributions. This suppression now underestimates the measured asymmetry at 44 MeV/nucleon. The quadrupole matrix elements need to be scaled by 1.6 to restore agreement with the data. The importance of the $E2$ contributions and higher-order effects falls with increasing incident energy and the data near 80 MeV/nucleon add little to the clarification of the $E2$ component. It will still be useful, however, to appply our partial-wave CDCC analysis to the forthcoming momentum distributions from GSI, measured at 250 MeV/nucleon, as in Ref. [12].

In summary, ^{8}B breakup data are now available over a

wide energy range. The data at 26 MeV, from Notre Dame [27], are well described by the CDCC and single-particle-model $E\lambda$ strengths, although the error bars on these data are significant. Predictions for the parallel momentum distribution data from the NSCL at higher energies, particularly the data at 44.1 MeV/nucleon, show considerable reaction model dependence, the CDCC predicting large higher-order effects and a corresponding suppression of $E2$ interference.

We have shown that a theoretical description of the ^{8}B breakup process exists that reproduces the asymmetry seen in all the available (40–80)-MeV/nucleon ^{8}B breakup data sets on Ag and Pb targets, with a consistent (enhanced) $E2$ strength. However, large (and unphysical) changes to the single-particle structure model would be required to increase the $E2$ amplitude by the factor of 1.6 required to reinstate the observed asymmetries. It remains to be clarified if this reveals a difficulty with the ^{8}B structure, the CDCC convergence, or with the data themselves.

It would be timely, as a first step toward such a theoretical clarification, to carry out detailed comparisons of the results of the available (CDCC and time-dependent) higher-order reaction theories, in particular for pure Coulomb breakup where both methods should be accurate. The very interesting case of the 44.1-MeV NSCL $p_{\|}$ data offers an energy and angular regime in which the assumptions underlying both theories are expected to be quite reliable and where these comparisons should be very informative. It is likely, however, that the assumption that ^{8}B can be satisactorily described using a pure $p_{3/2}$ single-particle model is at fault. Core state mixing in the ^{8}B ground state, as well as dynamical core excitations, will need to be considered in future calculations.

ACKNOWLEDGMENTS

This work was supported by the United Kingdom Engineering and Physical Sciences Research Council (EPSRC) through Grant No. GR/M82141. The authors would like to thank Dr. Barry Davids for providing the data used here in tabular form and for his valuable comments on an earlier draft of this paper.

[1] G. Baur and H. Rebel, J. Phys. G **20**, 1 (1994); Annu. Rev. Nucl. Part. Sci. **46**, 321 (1996).
[2] F.J. Vaughn, R.A. Chalmers, D. Khohler, and L.F. Chase, Jr., Phys. Rev. C **2**, 1657 (1970).
[3] B.W. Filippone, A.J. Elwyn, C.N. Davids, and D.D. Koetke, Phys. Rev. Lett. **50**, 412 (1983); Phys. Rev. C **28**, 2222 (1983).
[4] P.D. Parker, Phys. Rev. **150**, 851 (1966).
[5] R.W. Kavanagh, T.A. Tombrello, J.M. Mosher, and D.R. Goosman, Bull. Am. Phys. Soc. **14**, 1209 (1969).
[6] C. Wiezorek, H. Krawinkel, R. Santo, and L. Wallek, Z. Phys. A **282**, 121 (1977).
[7] F. Strieder *et al.*, Z. Phys. A **355**, 209 (1996).
[8] F. Hammache *et al.*, Phys. Rev. Lett. **86**, 3985 (2001).
[9] A.R. Junghans *et al.*, Phys. Rev. Lett. **88**, 041101 (2002).
[10] T. Motobayashi *et al.*, Phys. Rev. Lett. **73**, 2680 (1994).
[11] T. Kikuchi *et al.*, Phys. Lett. B **391**, 261 (1997).
[12] N. Iwasa *et al.*, Phys. Rev. Lett. **83**, 2910 (1999).
[13] B. Davids *et al.*, Phys. Rev. Lett. **86**, 2750 (2001).
[14] B. Davids, S.M. Austin, D. Bazin, H. Esbensen. B.M. Sherrill, I.J. Thompson, and J.A. Tostevin, Phys. Rev. C **63**, 065806 (2001).
[15] K. Langanke and T.D. Shoppa, Phys. Rev. C **49**, R1771 (1994).
[16] S. Typel and G. Baur, Phys. Rev. C **50**, 2104 (1994).
[17] M. Gai and C.A. Bertulani, Phys. Rev. C **52**, 1706 (1995).
[18] H. Esbensen and G.F. Bertsch, Nucl. Phys. **A600**, 37 (1996).
[19] B. Davids *et al.*, Phys. Rev. Lett. **81**, 2209 (1998).
[20] J.H. Kelley *et al.*, Phys. Rev. Lett. **77**, 5020 (1996).
[21] H. Esbensen, in *International School of Heavy-Ion Physics, 4th Course: Exotic Nuclei*, edited by R.A. Broglia and P.G. Hansen (World Scientific, Singapore, 1998), p. 71.
[22] H. Esbensen, G.F. Bertsch, and C.A. Bertulani, Nucl. Phys. **A581**, 107 (1995).
[23] S. Typel, H.H. Wolter, and G. Baur, Nucl. Phys. **A613**, 147 (1997).
[24] V.S. Melezhik and D. Baye, Phys. Rev. C **59**, 3232 (1999).
[25] S. Typel and R. Shyam, Phys. Rev. C **64**, 024605 (2001).
[26] J.A. Tostevin, F.M. Nunes, and I.J. Thompson, Phys. Rev. C **63**, 024617 (2001).
[27] J.J. Kolata, V. Guimarães, D. Peterson, P. Santi, R.H. White-Stevens, S.M. Vincent, F.D. Becchetti, M.Y. Lee, T.W. O'Donnell, D.A. Roberts, and J.A. Zimmerman, Phys. Rev. C **63**, 024616 (2001).
[28] F.C. Barker, Aust. J. Phys. **33**, 177 (1980).
[29] R.G. Robertson, Phys. Rev. C **7**, 543 (1973).
[30] C.A. Bertulani, Phys. Rev. C **49**, 2688 (1994).
[31] T.A. Tombrello, Nucl. Phys. **71**, 459 (1965).
[32] K.H. Kim, M.H. Park, and B.T. Kim, Phys. Rev. C **35**, 363 (1987).
[33] F.M. Nunes, R. Crespo, and I.J. Thompson, Nucl. Phys. **A615**, 69 (1997).
[34] N.K. Timofeyuk, Nucl. Phys. **A620**, 29 (1997).
[35] B.A. Brown, A. Csótó, and R. Sherr, Nucl. Phys. **A597**, 66 (1996).
[36] B.A. Brown, P.G. Hansen, B.M. Sherrill, and J.A. Tostevin, Phys. Rev. C **65**, 061601(R) (2002).
[37] L.V. Grigorenko, B.V. Danilin, V.D. Efros, N.B. Shul'gina, and M.V. Zhukov, Phys. Rev. C **57**, R2099 (1998); **60**, 044312 (1999).
[38] D. Cortina-Gil *et al.*, Phys. Lett. B **529**, 36 (2002).
[39] M. Kamimura, M. Yahiro, Y. Iseri, H. Kameyama, Y. Sakuragi, and M. Kawai, Prog. Theor. Phys. Suppl. **89**, 1 (1986); N. Austern, Y. Iseri, M. Kamimura, M. Kawai, G. Rawitscher, and M. Yahiro, Phys. Rep. **154**, 125 (1987).
[40] J.S. Al-Khalili and J.A. Tostevin, in *Scattering: Scattering and Inverse Scattering in Pure and Applied Science*, edited by E.R. Pike and Pierre C. Sabatier (Academic, London, 2001), Chap. 3.1.3.

[41] I.J. Thompson, Comput. Phys. Rep. **7**, 167 (1988); FRESCO users' manual, University of Surrey, UK.
[42] R. Shyam and I.J. Thompson, Phys. Rev. C **59**, 2645 (1999).
[43] F.M. Nunes and I.J. Thompson, Phys. Rev. C **59**, 2652 (1999).
[44] H. Fuchs, Nucl. Instrum. Methods Phys. Res. **200**, 361 (1982).
[45] J. Cook, Nucl. Phys. **A490**, 153 (1982).
[46] F.D. Becchetti and G.W. Greenlees, Phys. Rev. **182**, 1190 (1969).